Constraints on the nuclear equation of state from nuclear masses and radii in a Thomas-Fermi meta-modeling approach

D. Chatterjee,[1,*] F. Gulminelli,[1,†] Ad. R. Raduta,[2,‡] and J. Margueron[3,4,§]

[1]*LPC, UMR6534, ENSICAEN, F-14050 Caen, France*

[2]*IFIN-HH, P.O. Box MG6, Bucharest-Magurele, Romania*

[3]*Institute for Nuclear Theory, University of Washington, Seattle, Washington 98195, USA*

[4]*Institut de Physique Nucléaire de Lyon, CNRS/IN2P3, Université de Lyon, Université Claude Bernard Lyon 1, F-69622 Villeurbanne Cedex, France*

(Received 31 August 2017; revised manuscript received 15 November 2017; published 18 December 2017)

The question of correlations among empirical equation of state (EoS) parameters constrained by nuclear observables is addressed in a Thomas-Fermi meta-modeling approach. A recently proposed meta-modeling for the nuclear EoS in nuclear matter is augmented with a single finite size term to produce a minimal unified EoS functional able to describe the smooth part of the nuclear ground state properties. This meta-model can reproduce the predictions of a large variety of models, and interpolate continuously between them. An analytical approximation to the full Thomas-Fermi integrals is further proposed giving a fully analytical meta-model for nuclear masses. The parameter space is sampled and filtered through the constraint of nuclear mass reproduction with Bayesian statistical tools. We show that this simple analytical meta-modeling has a predictive power on masses, radii, and skins comparable to full Hartree-Fock or extended Thomas-Fermi calculations with realistic energy functionals. The covariance analysis on the posterior distribution shows that no physical correlation is present between the different EoS parameters. Concerning nuclear observables, a strong correlation between the slope of the symmetry energy and the neutron skin is observed, in agreement with previous studies.

DOI: 10.1103/PhysRevC.96.065805

I. INTRODUCTION

The nuclear equation of state (EoS) is one of the fundamental entities that governs the behavior of nuclear systems, from terrestrial nuclei to neutron stars [1]. However, astrophysical observations alone cannot provide enough information to constrain the behavior of asymmetric nuclear matter in the different density and isospin asymmetry domains, and the best knowledge of the EoS still comes from low energy nuclear physics experiments, i.e., nuclear ground state properties such as masses and radii of nuclei or the neutron skin, among others [2,3].

For this reason, extracting reliable confidence intervals for the EoS empirical parameters from the laboratory data has become a crucial issue in compact star modeling. Thanks to the new developments in density functional theory (DFT), in *ab initio* modeling, and thanks to the large number of data on asymmetric nuclei collected from the new rare-ion beam facilities worldwide, enormous progress was achieved in the past decade [4–10].

Within a specific functional family, confidence intervals for the EoS parameters can be extracted [8,11,12] using standard Bayesian statistical tools [13], but the problem of the model dependence of the results naturally arises. This model dependence is responsible for the fact that the correlations among empirical parameters are modified by changing the functional family, from Skyrme to Gogny or Relativistic Mean Field (RMF) or Relativistic Hartree-Fock (RHF) [14–18]. A simple example is given by nonrelativistic functionals: it is easy to show analytically that the phenomenological density dependent term of Skyrme interactions, the t_3 term, induces artificial correlations among the different isoscalar as well as isovector EoS terms [16]. A possible solution of this problem was proposed in Ref. [17]. In that paper, a meta-modeling for the nuclear equation of state is introduced, as a representation of the class of continuous EoS models (that is, models assuming that there is no discontinuity at high density, possibly induced by a first-order phase transition for instance) [19]. The meta-model consists of a functional which is flexible enough that it can reproduce within its parameter space the different functionals obtained from most of the existing models (relativistic, nonrelativistic, *ab initio*). Varying the parameters of the meta-model thus allows exploration of a large class of continuous EoS models, and continuously interpolating between them. The prior distribution of the meta-model parameters is extracted from a compilation of the different models belonging to the class. Using Bayesian statistics [20], posterior distributions can be obtained by filtering the meta-model parameter space with the constraint of reproducing physical observables. The resulting EoS and observable predictions can then be seen as weighted averages of the different models, where the artificial parameter correlations induced by the choice of a given model are naturally suppressed. A first application of this technique was proposed in Ref. [21], where astrophysical observables from neutron star physics were analyzed.

In this paper we want to extend the study of Ref. [21] by analyzing some observables from finite nuclei, namely

*dchatterjee@lpccaen.in2p3.fr

†gulminelli@lpccaen.in2p3.fr

‡araduta@nipne.ro

§j.margueron@ipnl.in2p3.fr

nuclear masses and radii. However, a difficulty comes from the fact that the energy functionals used to describe ground state nuclear properties contain many more parameters than the ones entering the EoS of infinite nuclear matter, such as (at least) effective masses, surface, spin-orbit, and tensor terms, and building up a meta-model that includes all this complexity is highly nontrivial. A meta-model of nuclear structure is not only hard to conceive, but also redundant for the purpose of determining the nuclear EoS. Indeed, the proliferation of extra parameters, though essential to pin down the complexity of nuclear structure, makes it hard to sort out the specific effect of EoS parameters on a given nuclear observable [14]. To give an example, this problem is shown by different recent works analyzing the EoS dependence of the neutron skin in ^{208}Pb. Based on a droplet model analysis, the Barcelona group [22] has shown that the skin is not directly correlated to the EoS parameter $L_{\rm sym}$ (slope of the symmetry energy at saturation), but rather to the ratio $L_{\rm sym}/Q$, where Q represents the so-called surface stiffness parameter, which is related to the differential surface tension between protons and neutrons. Consequently, one can expect that the EoS independent surface contribution to the skin should be sorted out in order to recover the correct correlation with the EoS. However, when using more sophisticated EoS models it was shown [18,23,24] that the surface contribution is remarkably constant in the different relativistic and nonrelativistic models, and therefore the correlation of the skin with $L_{\rm sym}$ is preserved. It was conjectured [23] that this constant behavior might come from the constraint on nuclear mass reproduction applied to the DFT functionals, but the argument neglects the fact that the mass itself is known to provide constraints on the EoS [4,10,25] besides the constraints on the finite size parameters [26].

For this reason, we limit ourselves to the extended Thomas-Fermi (ETF) approximation. In the Thomas-Fermi approximation, the ground state energy functional of a finite nucleus is simply given by the functional for homogeneous nuclear matter (that is, the EoS model), calculated at the local density which is variationally determined. Our Thomas-Fermi meta-model will therefore be given by the same meta-functional introduced in nuclear matter in Refs. [17,21], augmented by a single isoscalar surface term, which can be taken as an effective representation of finite size effects. Varying the parameters of the meta-model within reasonable priors, we will therefore generate all the possible mass models associated with the different DFT functionals, when the ground state of these models is calculated in the spherical ETF approximation.

We show that considering the first low order parameters is sufficient to pin down the full isoscalar and isovector behavior of the smooth part of the nuclear binding energy, and the predictive power of the meta-model is not significantly improved if further parameters are added.

The addition of a single finite size term, subject to the constraint of correctly reproducing experimental nuclear mass, allows us to single out the interplay between bulk and surface parameters. A similar strategy was recently employed in Ref. [27] and shown to be able to reproduce, with high accuracy, a series of nuclear observables including binding energies, two-neutron and two-proton separation energies, and charge radii.

With this meta-modeling, we will then sample the multidimensional parameter space with a prior flat distribution, and filter the parameter set through the constraint of least-square mass reproduction. This allows us to explore the possible physical correlations among empirical parameters and carry out a systematic investigation of radii and neutron skins in nuclei. We will show that the slope of symmetry energy strongly correlates with the neutron skin, and its measurement is virtually unaffected by the uncertainty in any of the other empirical quantities, thus highlighting the importance of neutron skin in the determination of the nuclear EoS [28–30].

II. FORMALISM

In this section, we shortly review the formalism of meta-modeling for uniform nuclear matter. Then we detail its implementation in finite nuclei in the framework of the Extended Thomas-Fermi (ETF) approximation. Finally an analytical solution of the Thomas-Fermi integrals is explicitly worked out, giving an effective analytical meta-model for nuclear mass with coefficients directly related to the empirical parameters of nuclear matter.

A. Energy functional for homogeneous matter

Following Ref. [17], the description of homogeneous nuclear matter is based on a metamodeling belonging to the class of continuous EoS models. Within this meta-model, the EoS coefficients are directly related to the state-of-the-art knowledge of nuclear matter based on data from nuclear experiments. The energy per particle in asymmetric nuclear matter can be separated into isoscalar and isovector channels as

$$e(n_0,\delta) = e_{IS}(n_0) + \delta^2 e_{IV}(n_0). \tag{1}$$

Here, $\delta = n_1/n_0$ is the asymmetry of bulk nuclear matter, the density $n_0 = n_n + n_p$ ($n_1 = n_n - n_p$) being the sum (difference) of proton and neutron densities n_p and n_n. In principle the expansion in asymmetry parameter δ in Eq. (1) can go up to any even power of δ, due to isospin symmetry. In practice stopping at order δ^2 is usually enough [17] for the potential part. Nonquadraticities in the kinetic part are treated explicitly; see below. The empirical parameters appear as the coefficients of the series expansion around saturation density $n_{\rm sat}$ in terms of a dimensionless parameter $x = (n_0 - n_{\rm sat})/(3n_{\rm sat})$, i.e.,

$$e_{IS} = E_{\rm sat} + \tfrac{1}{2}K_{\rm sat}x^2 + O(x^3), \tag{2}$$

$$e_{IV} = E_{\rm sym} + L_{\rm sym}x + \tfrac{1}{2}K_{\rm sym}x^2 + O(x^3). \tag{3}$$

The isoscalar channel is written in terms of the energy per particle at saturation, $E_{\rm sat}$, and the isoscalar incompressibility $K_{\rm sat}$. There is no linear term in x since the pressure is zero at saturation density. The isovector channel is defined in terms of the symmetry energy $E_{\rm sym}$ and its first two derivatives $L_{\rm sym}$, $K_{\rm sym}$. In principle, there is an infinite number of terms in the series expansion. To reproduce well the equation of state and its derivatives of the different models described by the meta-model up to $4n_{\rm sat}$, it is enough to stop at order 4 in x [17]. For our purpose, since we are only interested in finite nuclei, around and below saturation density, it is sufficient to stop at order 2 in x [17]. Therefore, in this study, which is

uniquely centered on nuclear ground state properties, we do not consider higher order terms.

To achieve a good representation of the different models at low density and large isospin asymmetries, the density dependence of the kinetic energy term is separated from that of the potential term:

$$e(x,\delta) = e_{\rm kin}(x,\delta) + e_{\rm pot}(x,\delta). \tag{4}$$

The kinetic energy term is written as

$$e_{\rm kin} = t_{\rm sat}^{FG}(1+3x)^{2/3}\frac{1}{2}\left[(1+\delta)^{5/3}\frac{m}{m_n^*} + (1-\delta)^{5/3}\frac{m}{m_p^*}\right], \tag{5}$$

where the constant $t_{\rm sat}^{FG}$ is given by

$$t_{\rm sat}^{FG} = \frac{3}{5}\frac{\hbar^2}{2m}\left(\frac{3\pi^2}{2}\right)^{2/3} n_{\rm sat}^{2/3}, \tag{6}$$

and m_n^* and m_p^* are the in-medium masses of protons and neutrons, m being the bare nucleon mass. The in-medium effective mass can also be expanded in terms of the density parameter x as [17]

$$\frac{m}{m_q^*} = 1 + (\kappa_{\rm sat} + \tau_3\kappa_{\rm sym}\delta)\frac{n_0}{n_{\rm sat}}, \tag{7}$$

where $\tau_3 = 1$ for neutrons and -1 for protons.

This expansion adds two extra empirical parameters to our parameter set, namely

$$\begin{aligned}\kappa_{\rm sat} &= m/m_{\rm sat} - 1,\\ \kappa_{\rm sym} &= \tfrac{1}{2}[m/m_n^*(x=0,\delta=1) - m/m_p^*(x=0,\delta=1)].\end{aligned} \tag{8}$$

Here, $\kappa_{\rm sat}$ is related to the isoscalar effective mass and $\kappa_{\rm sym}$ is half the difference of the inverse of the effective masses in neutron matter. More commonly, the isovector dependence of the effective mass is described in terms of the isospin splitting of the nucleon masses in neutron matter,

$$\begin{aligned}\frac{\Delta m^*}{m} &= \tfrac{1}{2}[m_n^*(x=0,\delta=1) - m_p^*(x=0,\delta=1)].\\ &= \frac{\kappa_{\rm sym}}{(\kappa_{\rm sym})^2 - (1+\kappa_{\rm sat})^2}.\end{aligned} \tag{9}$$

The value of $\Delta m^*/m$ is not very well constrained from experimental data [31]. Theoretical predictions based on the Bruckner-Hartree-Fock formalism prefer a small value, of the order of 0.1 [31]. In this work, we fix $\kappa_{\rm sym} = 0$ since this parameter has a very weak effect for masses of finite nuclei.

Similarly, we write the potential part of the energy per particle as a series expansion separated into isoscalar and isovector contributions $a_{\alpha 0}$ and $a_{\alpha 2}$, up to second order in the parameter x as follows:

$$e_{\rm pot} = \sum_{\alpha=0}^{2}(a_{\alpha 0} + a_{\alpha 2}\delta^2)\frac{x^\alpha}{\alpha!}u_\alpha(x)\,. \tag{10}$$

This expression for the potential term corresponds to the meta-modeling ELFc (Empirical Local density Functional, with correction at zero density) of Ref. [17]. The function u is defined as $u_\alpha(x) = 1 + 27x^3e^{-b(3x+1)}$ such that $e_{\rm pot}$ satisfies the following limit: $e_{\rm pot} \to 0$ for $n_0 \to 0$. The parameter b is set to $b = 10\ln 2$ such that it has a negligible contribution above saturation density; see Ref. [17] for more details.

Then comparing with Eqs. (2) and (3), the isoscalar and isovector coefficients in the expansion can be written in terms of the empirical parameters as [17]

$$a_{00} = E_{\rm sat} - t_{\rm sat}^{FG}(1+\kappa_{\rm sat}), \tag{11}$$

$$a_{10} = -t_{\rm sat}^{FG}(2+5\kappa_{\rm sat}), \tag{12}$$

$$a_{20} = K_{\rm sat} - 2t_{\rm sat}^{FG}(-1+5\kappa_{\rm sat}), \tag{13}$$

$$a_{02} = E_{\rm sym} - \frac{5}{9}t_{\rm sat}^{FG}(1+\kappa_{\rm sat}), \tag{14}$$

$$a_{12} = L_{\rm sym} - \frac{5}{9}t_{\rm sat}^{FG}(2+5\kappa_{\rm sat}), \tag{15}$$

$$a_{22} = K_{\rm sym} - \frac{10}{9}t_{\rm sat}^{FG}(-1+5\kappa_{\rm sat}). \tag{16}$$

A given choice for the parameter set $\{E_{\rm sat}, n_{\rm sat}, K_{\rm sat}, E_{\rm sym}, L_{\rm sym}, K_{\rm sym}, \kappa_{\rm sat}\}$ defines a possible realization of the meta-model, and a full exploration of the seven-dimensional parameter space ensures, below saturation, a quasicomplete mapping of the possible models belonging to the class of continuous EoS with the exclusion of models considering an effective mass splitting, because of the simplification $\kappa_{\rm sym} = 0$. The parameter set will be denoted as $\{P_\alpha\}$ in the following.

B. Energy functional for nuclei

1. The ETF approximation

To extend the formalism of Sec. II A to finite nuclei, we employ the spherical ETF approximation. The resulting meta-modeling will be called "ETF meta-functional" in the following. In this approximation, the mass of a finite nucleus is obtained performing a numerical integration of the local energy functional folded with a parametrized density profile, according to

$$E_{\rm tot}(A,\delta) = 4\pi\int_0^\infty dr\, r^2(\mathcal{H}_{ETF}[n_p,n_n] + \mathcal{H}_{\rm coul}[n_p]). \tag{17}$$

The energy functional is given by the meta-modeling presented in Sec. II A, complemented with a gradient term to account for finite size effects [27]. In the framework of the ETF theory, an extra gradient term arises from the semiclassical $\hbar$ expansion of the nonlocal momentum operator. The final result at the second order in $\hbar$ is given by

$$\mathcal{H}_{ETF}[n_n,n_p] = e(n_n,n_p)n_0 + \sum_{q=n,p}\frac{\hbar^2}{2m_q^*}\tau_{2q} + C_{\rm fin}(\nabla n_0)^2. \tag{18}$$

Here, the energy per particle of uniform nuclear matter e and the effective masses m_q^* are given by Eqs. (4) and (7). The second-order local and nonlocal corrections $\tau_{2q} = \tau_{2q}^l + \tau_{2q}^{nl}$

are given by the $\hbar$ expansion as

$$\tau^{l}_{2q} = \frac{1}{36}\frac{(\nabla n_q)^2}{n_q} + \frac{1}{3}\Delta n_q \tag{19}$$

$$\tau^{nl}_{2q} = \frac{1}{6}\frac{\nabla n_q \nabla f_q}{f_q} + \frac{1}{6}n_0\frac{\Delta f_q}{f_q} - \frac{1}{12}n_q\left(\frac{\nabla f_q}{f_q}\right)^2, \tag{20}$$

with $f_q = m/m^*_q$. Finally, the $C_{\rm fin}$ term is the extra isoscalar surface coupling. To have a complete meta-model description of the different DFT functionals for finite nuclei in the ETF approximation, in principle many different gradient terms should be introduced. However, as discussed in the Introduction, the extra functional terms are largely redundant if we only aim at calculating masses and radii, and we only consider this minimal extension of the meta-functional in the present paper.

The density profiles are taken as Fermi functions,

$$n_q(r) = n_{{\rm bulk},q}F_q(r), \quad F_q(r) = (1 + e^{(r-R_q)/a_q})^{-1}, \tag{21}$$

R_q are effective radii fixed by particle number conservation, and the parameters $n_{{\rm bulk},q}$ and a_q are treated as four independent variational variables. The minimization with respect to these variables is performed including the direct and exchange Coulomb terms at the level of the energy density defined as [32]

$$\mathcal{H}_{\rm coul}[n_p] = 2\pi e^2 n_p(r)\int_0^r dr' n_p(r')\left(\frac{r'^2}{r} - r'\right) - \frac{3e^2}{4}\left(\frac{3}{\pi}\right)^{1/3} n_p^{4/3}(r), \tag{22}$$

where the Slater approximation has been employed to estimate the exchange Coulomb energy density.

2. Analytical mass model

The ETF approximation of Sec. II B 1 is a straightforward extension of the meta-model of Sec. II A suited to evaluate nuclear ground state properties. However, the variational determination of the density profile parameters is numerically very demanding when the systematic exploration of the huge parameter space of the meta-functional is performed. For this reason, we have developed an analytical approximation of the ETF integrals. The theoretical method is described in detail in Refs. [33,34] in the case of a Skyrme functional. Here we only give the main results and the differences of the present study with respect to [33,34], arising from the use of the meta-functional instead of the Skyrme functional. The density profiles are still given by Eq. (21), but the parameters $n_{{\rm bulk},q}$, a_q are now analytically determined.

The parameters $n_{{\rm bulk},q}$ can be obtained from the infinite matter limit of the Euler-Lagrange variational equations [35] as the proton and neutron saturation densities [36]: $n_{{\rm bulk},q} = n_{\rm bulk}(\delta)(1 \pm \delta)/2$, where the saturation density for asymmetric matter depends on the asymmetry δ and can be written as a function of the empirical parameters as [36]

$$n_{\rm bulk}(\delta) = n_{\rm sat}\left(1 - \frac{3L_{\rm sym}\delta^2}{K_{\rm sat} + K_{\rm sym}\delta^2}\right). \tag{23}$$

If we further assume $a_n = a_p = a$, the diffuseness of the density profile can be analytically determined by energy minimization, giving [34]

$$a^2(A,\delta) = \frac{\mathcal{C}^{NL}_{\rm surf}(\delta)}{\mathcal{C}^{L}_{\rm surf}(\delta)} + \Delta R_{HS}(A,\delta) \times \sqrt{\frac{\pi}{\left(1 - \frac{K_{1/2}}{18J_{1/2}}\right)}}\frac{n_{\rm sat}}{n_{\rm bulk}(\delta)}\frac{3J_{1/2}}{\mathcal{C}^{L}_{\rm surf}(\delta)}\sqrt{\frac{\mathcal{C}^{NL}_{\rm surf}(0)}{\mathcal{C}^{L}_{\rm surf}(0)}}(\delta - \delta^2). \tag{24}$$

In this expression, the coefficients $J_{1/2}$ and $K_{1/2}$ represent the value of the symmetry energy and its curvature at one half of the saturation density, $J_{1/2} = 2e_{IV}(n_{\rm sat}/2)$, $K_{1/2} = 18(\frac{n_{\rm sat}}{2})^2\partial^2 e_{IV}/\partial n^2|_{n_{\rm sat}/2}$, and

$$\Delta R_{HS} = \left(\frac{3}{4\pi}\right)^{1/3}\left[\left(\frac{A}{n_{\rm bulk}(\delta)}\right)^{1/3} - \left(\frac{Z}{n_{{\rm bulk},p}(\delta)}\right)^{1/3}\right] \tag{25}$$

is the difference between the hard sphere radius $R_{HS} = r_{\rm bulk}(\delta)A^{1/3}$ and the proton radius $R_{HS,p} = r_{{\rm bulk},p}(\delta)Z^{1/3}$ in the hard sphere limit.

One should observe that the approximation $a_n = a_p$ employed to obtain Eq. (24) is not verified in complete variational ETF or HF calculations of asymmetric nuclei; see for instance Refs. [37,38]. It was indeed suggested that a substantial fraction of the neutron skin is induced by the difference between a_n and a_p [22,23,37]. This effect corresponds to the nonbulk contribution to the neutron skin. In our model, however, we can see from Eq. (24) that, due to the complex isospin dependence of the ETF functional, the diffuseness a explicitly contains isovector nonbulk contributions generated by the non-local terms. We will see in Sec. IV D that even within the approximation $a_n = a_p$ the skin in our model acquires a finite surface contribution. While not being explicitly in contradiction with the arguments presented in Refs. [22,23,37], our meta-modeling shows that the richness of the mean field induces sometimes more features than *a priori* expected.

Finally, the asymmetry parameter δ is defined in the framework of the droplet model as [39]

$$\delta = \frac{I + \frac{3a_c Z^2}{8QA^{5/3}}}{1 + \frac{9E_{\rm sym}}{4QA^{1/3}}}, \tag{26}$$

where $a_c = 3e^2/[20\pi\epsilon_0 r_{\rm bulk}(\delta)]$ is the Coulomb parameter and $r_{\rm bulk}(\delta) = [\frac{4}{3}\pi n_{\rm bulk}(\delta)]^{-1/3}$ the mean radius per nucleon. More details can be found in Refs. [33,34,40].

3. Energy calculation

Using the analytical density profiles Eq. (21), the nuclear part of the integral Eq. (17) can be analytically evaluated, with some approximation [33,34]. This allow us to decompose the total energy into a bulk and a surface contribution:

$$E_{\rm nuc}(A,\delta) = E_b + E_s. \tag{27}$$

The bulk energy is the equilibrium energy of homogeneous nuclear matter at isospin δ,

$$E_b(A,\delta) = e(n_{\rm bulk}(\delta),\delta)A, \tag{28}$$

where e is defined in Eq. (4). The surface energy E_s contains contributions from the gradient terms in the energy functional. It can be further decomposed into an isoscalar and an isovector part,

$$E_s(A,\delta) = E_s^{IS} + E_s^{IV}\delta^2. \tag{29}$$

Thanks to the Fermi profile ansatz, the integration of the isoscalar part is fully analytical, giving [33,34]

$$\begin{aligned} E_s^{IS} &= \left[\mathcal{C}^L_{\rm surf}(\{P_\alpha\}) + \mathcal{C}^{NL}_{\rm surf}(\{P_\alpha\},C_{\rm fin})\right]\frac{a}{r_{\rm bulk}}A^{2/3} \\ &+ \left[\mathcal{C}^L_{curv}(\{P_\alpha\}) + \mathcal{C}^{NL}_{curv}(\{P_\alpha\},C_{\rm fin})\right]\left[\frac{a}{r_{\rm bulk}}\right]^2 A^{1/3} \\ &+ \left[\mathcal{C}^L_{\rm ind}(\{P_\alpha\}) + \mathcal{C}^{NL}_{\rm ind}(\{P_\alpha\},C_{\rm fin})\right]\left[\frac{a}{r_{\rm bulk}}\right]^3, \end{aligned} \tag{30}$$

where the explicit expressions for the $\mathcal{C}^{L/NL}_{\rm surf/curv/ind}$ coefficients are given in Refs. [33,34].

We can see that the surface energy consists of a surface, a curvature, and a constant term [39]. In turn, these terms can be separated into a local and a non-local part. The local terms depend only on the bulk density $n_{\rm bulk}$ and on the empirical EoS parameters $\{P_\alpha\}$ [we recall that $n_{\rm bulk}$ depends only on the isospin parameter δ and on the empirical $\{P_\alpha\}$ set; see Eq. (23)]. The nonlocal part also depends on the gradient terms and thus on the finite size parameter ($C_{\rm fin}$, in the present application). It is also interesting to remark that the isospin dependence of the surface energy is more complex than in the usual parabolic approximation, and the expression (29) effectively contains higher orders in δ because of the δ dependence of the diffuseness a_q, saturation radius $r_{\rm bulk}$, and of the saturation density $n_{\rm bulk}$.

The isovector surface part can be evaluated in the Gaussian approximation as [34]

$$E_s^{IV} = E^{IV}_{\rm surf}A^{2/3} + E^{IV}_{\rm ind}\,, \tag{31}$$

where again the coefficients only depend on the EoS parameters, $E_{\rm surf}(\{P_\alpha\},n_{\rm bulk}(\delta))$, $E_{\rm ind}(\{P_\alpha\},n_{\rm bulk}(\delta))$. It was shown in Ref. [34] that this approximation to the surface symmetry energy gives a good reproduction of a full ETF calculation using the same density profiles, for isospin asymmetries up to $\delta \approx 0.3$ or $I \approx 0.4$, which are very close to the neutron drip line.

Finally, a Coulomb contribution is added to the total energy from Eqs. (30) and (31), which becomes

$$E_{\rm tot}(A,Z) = E_b(A,\delta) + E_s(A,\delta) + a_c\frac{Z^2}{A^{1/3}}\,. \tag{32}$$

4. Calculation of radii and skins

Within the same analytical ETF approximation, we can also calculate the root-mean-square (rms) radii of protons $\sqrt{\langle r_p^2\rangle}$ and neutrons $\sqrt{\langle r_n^2\rangle}$ as [23,36]

$$\langle r_q^2\rangle = \frac{3}{5}R^2_{HS,q}\left(1 + \frac{5\pi^2a^2}{6R^2_{HS,q}}\right)^2, \tag{33}$$

where the diffuseness a is given by Eq. (24). We can see from Eqs. (33) and (24) that the radii are explicitly correlated to $n_{\rm sat}$ through $r_{{\rm bulk},q}$ defining $R_{HS,q}$, but all the other isovector and isoscalar empirical parameters, including the finite size $C_{\rm fin}$, additionally enter in the radius definition. As discussed before, the radii are thus related to all empirical and surface parameters in a complex way.

The neutron skin is given by the difference in the rms radii of protons and neutrons, i.e., $\Delta R_{np} = \sqrt{\langle r_n^2\rangle} - \sqrt{\langle r_p^2\rangle}$. To compare with the observations, one must calculate the charge radius, which is related to the proton radius, using the relation

$$\langle r_{ch}^2\rangle^{1/2} = \left[\langle r_p^2\rangle + S_p^2\right]^{1/2},$$

where the correction $S_p = 0.8$ fm comes from the internal charge distribution of the proton [41,42].

With this fully analytical ETF meta-model, masses and radii can be evaluated for any arbitrary set of empirical parameters $\{P_\alpha\}$, provided an estimation of the extra finite size parameter $C_{\rm fin}$ is given. The determination of a confidence interval for this parameter is detailed in Sec. III.

III. FIXING A SET OF REFERENCE PARAMETERS

In the following, we vary the values of the EoS empirical parameters $\{P_\alpha\} \equiv \{n_{\rm sat}, E_{\rm sat}, \kappa_{\rm sat}, K_{\rm sat}, E_{\rm sym}, L_{\rm sym}, K_{\rm sym}\}$, as well as that of the effective finite size parameter $C_{\rm fin}$. From this variation, we study their influence on nuclear masses, isolate the best parameters from their ability to reproduce the experimental nuclear masses, and determine the correlations among the parameters within the constraints of the physical masses.

To reasonably restrict the huge space of the multi-dimensional prior parameter distribution, we need to know their average values and typical uncertainties. We extract a part of this information from a recent work where these data were compiled from a large number of Skyrme, relativistic mean field and relativistic Hartree-Fock models [17]. For each of them, the average and the standard deviation among the model predictions were estimated, and are reported in the second line of Table I. Alternatively, an optimized value of the empirical parameters can be estimated by a least-square fit of nuclear masses of some chosen nuclei with the full variational ETF, with resulting parameters also given in Table I (first line). From Table I we can see that the different approximations and optimization techniques lead to different values for the empirical parameters, as expected. The differences are, however, consistent with the standard deviations associated with the parameters in Ref. [17], also shown in the table (last line).

It is important to stress that, because of the possible correlations among empirical parameters, the set corresponding to the average values (second line of Table I) is not necessarily an optimized set, but only represents the central value of our prior

TABLE I. Empirical parameters used in the spherical ETF model, with different approximations (first and second lines). For comparison, the average and standard variation of the different parameters recommended in Ref. [17] is also given.

Parameter $\{P_\alpha\}$	$n_{\rm sat}$ (fm^{-3})	$E_{\rm sat}$ (MeV)	$K_{\rm sat}$ (MeV)	$E_{\rm sym}$ (MeV)	$L_{\rm sym}$ (MeV)	$K_{\rm sym}$ (MeV)	$m^*_{\rm sat}/m$	$C_{\rm fin}$ (MeV fm^5)
Full ETF, optimized set	0.1589	−15.84	266.73	32.81	58.37	−37.87	0.7484	62.15
Analytical ETF, reference set	0.1540	−16.04	255.91	33.43	77.92	−2.19	0.7	59
variation interval (absolute)	±0.0051	±0.20	±34.39	±2.64	±30.84	±142.71	±0.15	±13
variation interval (relative)	±3.31%	±1.25%	±13.44%	±7.90%	±39.58%	±6516.44%	±2.14%	±22.03%
Average $\langle\{P_\alpha\}\rangle$ (from Ref. [17])	0.155	− 15.8	230	32	60	−100	0.75	
Standard deviation σ_α (from Ref. [17])	±0.005	±0.3	±20	±2	±15	±100	±0.1	

parameter distribution. Still, we can use it as a reference set to determine a reasonable domain for the extra parameter $C_{\rm fin}$ which is specific to our meta-modeling and cannot therefore be taken from the literature.

We optimize $C_{\rm fin}$ by calculating the binding energy of symmetric nuclei with the analytical mass model, using for the other parameters the average empirical set from Table I. We minimize with respect to $C_{\rm fin}$ the average relative dispersion $\sum_{i=1}^{N}(E_{i,th} - E_{i,\rm exp})^2/E^2_{i,\rm exp}$, for the total number N of available nuclear masses, where the theoretical values E_{th} are calculated from the analytical ETF model Eq. (32), and the experimental values $E_{\rm exp}$ are taken from the AME2012 mass table [43]. The resulting value is $C_{\rm fin} = 59$ MeV fm^5. We call this parameter set EoS-$C_{\rm fin}$, as displayed in Fig. 1.

In realistic Skyrme functionals, other energy terms (spin-orbit, spin-gradient, isovector gradient terms) are added in addition to the surface term. To check whether a single effective isoscalar finite size term is sufficient to catch the information contained in nuclear masses, we introduce an additional spin-orbit term with coefficient C_{so} to the ETF functional Eq. (32), and minimize the average relative dispersion in the two-dimensional ($C_{\rm fin}$,C_{so}) space; see results EoS-$C_{\rm fin}$-C_{so} in Fig. 1. Though the optimal value of $C_{\rm fin}$ is obviously modified by the presence of the spin-orbit term (from $C_{\rm fin} = 59$ to $C_{\rm fin} = 61$ MeV fm^5), the quality of data reproduction is not modified as we can see from Fig. 1. This shows that this extra parameter is redundant as far as binding energies are concerned.

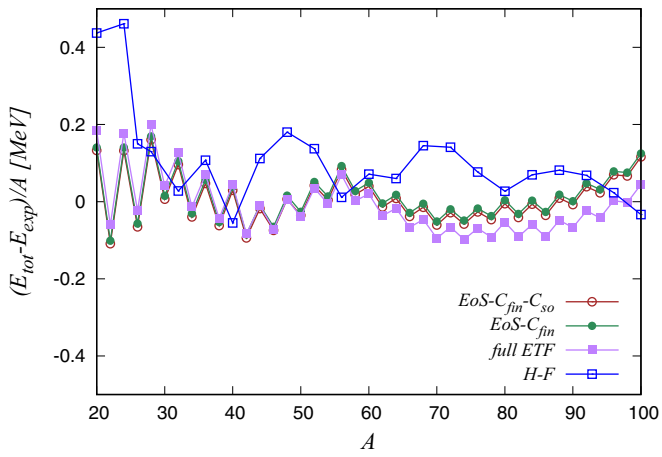

FIG. 1. Difference between theoretical and experimental energy per particle of symmetric nuclei for the reference analytical EoS, in the case where a single surface parameter $C_{\rm fin}$ is added to the empirical set (filled circles), and in the case where a spin-orbit coupling C_{so} is also added (open circles). The result for the full ETF using an optimized EoS (filled squares) and spherical Hartree-Fock results using the Sly4 [45] parameter set (open squares) are also given.

We can observe from Fig. 1 that the deviation of the ETF model from the experimental data is much higher than in full optimized DFT calculations; see for instance the best DFT in Ref. [44], where a residual difference between the DFT and the experimental total masses are of the order to 500 keV. Notice, however, that this excellent comparison is possible by introducing empirical corrections to the theoretical mass model. Without these corrections, the differences are larger and of the order of a few MeV. For reference, we show in Fig. 1 the comparison for the Skyrme Hartree-Fock (H-F) SLy4 mean field model, as well as the result of a full variational determination of the empirical parameters using the complete ETF with the empirical EoS, plus the extra $C_{\rm fin}$ term (see Sec. II B 1). We can see that both calculations show a performance comparable to the one of the analytical mass model, even if the absence of pairing in the ETF meta-modeling induces a spurious staggering as expected. One also obtains quantitatively similar results using other Skyrme interactions. This means that the observed deviation is not due to the limitations of the analytical mass model, but rather to the fact that we are working in the mean-field approximation and supposing spherical symmetry.

This comparison shows that our present ETF approximation is able to reproduce satisfactorily well the nuclear masses, averaging over shell corrections, and can be used further for extracting constraints and correlations among the empirical parameters.

The systematic error of the meta-modeling on symmetric nuclei can be very roughly estimated as $\Delta E \approx 100 \times A$ keV.

In our simplified functional, Eq. (18), the finite size term is purely isoscalar, while standard Skyrme functionals contain also isovector couplings. In order to test if such a term is needed for a reasonable reproduction of nuclear masses, we calculate the residuals for a large number of isotopic chains for $Z = 20$, 28, 50, and 82, using the $C_{\rm fin} = 59$ MeV fm^5 value extracted from the analysis of symmetric nuclei. The results are displayed in Fig. 2 and show that the residuals are of the same order for all asymmetries I. Again, the reproduction of experimental data is of comparable quality if the full ETF functional is used without approximations, using the optimized parameter set of Table I within the empirical model

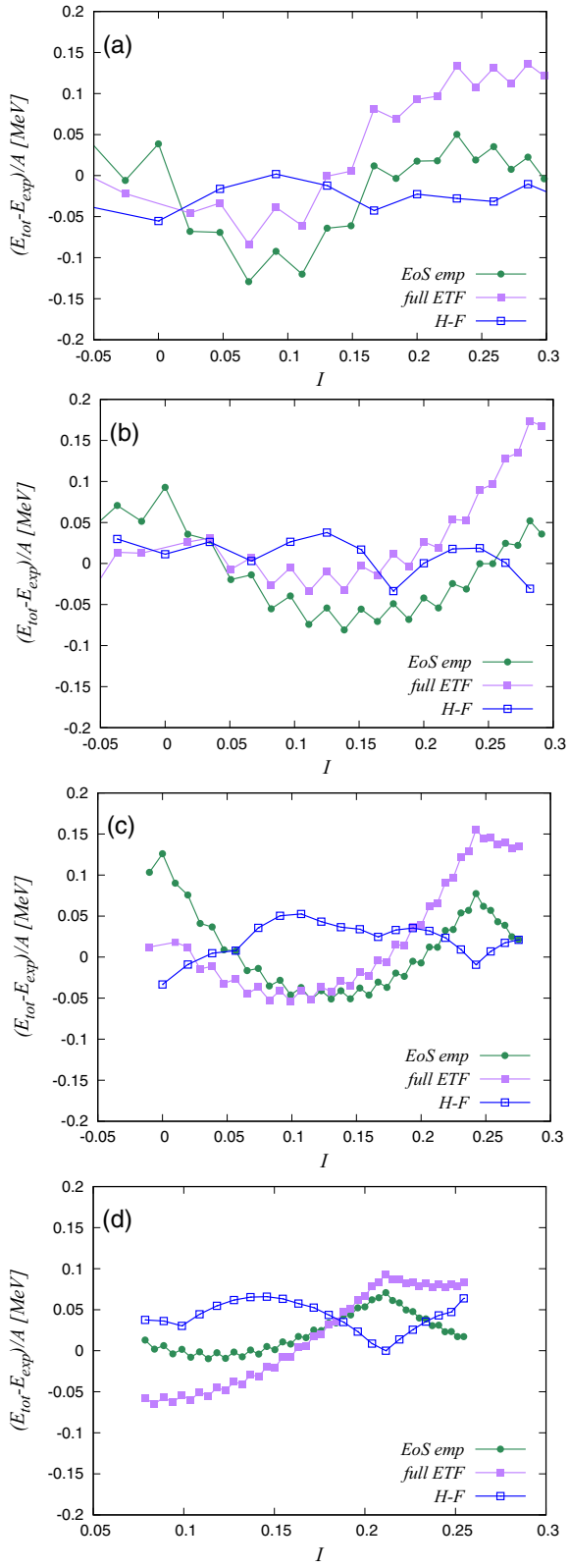

FIG. 2. Difference between theoretical and experimental energy per particle vs asymmetry $I = (N - Z)/A$ for different Z values: 20 (Ca), 28 (Ni), 50 (Sn), and 82 (Pb), for the reference empirical EoS (filled circles). The result for the full ETF mass model using an optimized EoS (filled squares) and spherical H-F results with the Sly4 parameter set (open squares) are also given.

(filled squares). Spherical HF calculations for even-even nuclei within the SLy4 parametrization [45] (empty squares) are also included in the figure. The presence of shell effects modifies the global shape of the residuals, but again the absolute value of the deviation is comparable. In the case of the full ETF, no surface isovector term is included, while this latter is taken into account in the SLy4 calculation.

We can conclude that the analytical ETF mass model leads to a systematic error on binding energies of the order of $\Delta E \approx 100 \times A$ keV, independent of the neutron richness. The introduction of an isovector surface parameter would not improve the predictive power of the meta-modeling, and a single isoscalar parameter is sufficient to reproduce the masses even along the full isotopic chains, within the precision allowed by the classical spherical ETF approximation, as already suggested in Ref. [27].

This somewhat surprising result might be due to the fact that within the ETF formalism the isovector surface energy depends in a nontrivial way on the EoS parameters and diffusivities, and is nonzero even without an isovector surface coupling [34].

The width of the prior distribution for the finite size parameter $C_{\rm fin}$ is estimated by varying $C_{\rm fin}$ in the analytical mass model such that the residuals $(E_{th} - E_{\rm exp})/A$ lie within $\pm$ 0.5 MeV, which leads to a value of $\Delta C_{\rm fin} \approx 13$ MeV fm^5. Concerning the set $\{P_\alpha\}$ of the EoS parameters, we vary them in the range $\langle P_\alpha\rangle - \sigma_\alpha \leqslant P_\alpha \leqslant \langle P_\alpha\rangle + \sigma_\alpha$, with averages and standard deviations from Table I.

To isolate the influence of the other empirical parameters $\{P_\alpha\}$ on the nuclear mass, we now vary each parameter individually and calculate the energy residuals for different symmetric nuclei and for the Sn isotopic chain. The summary of the effect on the energy residuals of variations of the empirical parameters, within error bars, is displayed in Fig. 3. Evidently, changing the isovector parameters $E_{\rm sym}, L_{\rm sym}, K_{\rm sym}$ does not affect the residuals for the symmetric case ($I = 0$). Therefore we plot only the influence of the isoscalar parameters on the energy residuals. We can see from Fig. 3 that all isoscalar parameters are individually correlated to the nuclear mass, and the largest effect is from m^*. As expected, the higher the isospin ratio I, the larger is the influence of isovector parameters. Very similar results are obtained, if the full ETF mass model is used, with variationally determined parameters for the density profile and consistent inclusion of the Coulomb energy in the variation (not shown).

The existence of such correlations does not necessarily mean that imposing a precise reproduction of nuclear mass will allow us to restrict the uncertainty domain of the empirical parameters, because the different parameters are *a priori* independent, and should therefore be independently varied. This we do in the next section.

IV. RESULTS

We now show the results obtained with the analytical and full ETF mass models employing the meta-functional. We recall that the parameters of the meta-functional are the set of empirical EoS parameters, complemented by the single parameter $C_{\rm fin}$ for the finite-size effect.

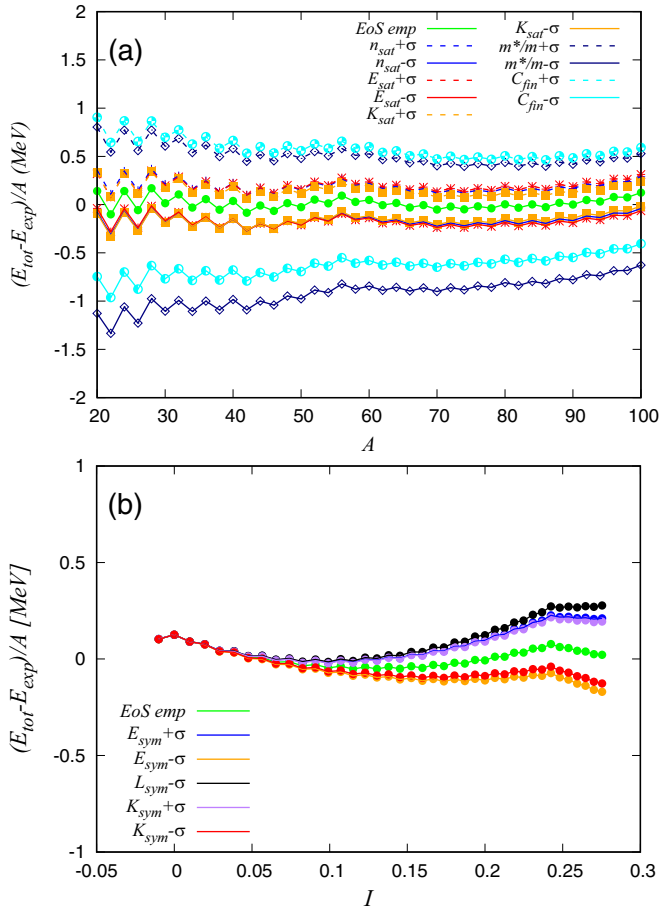

FIG. 3. Difference between theoretical and experimental binding energy per particle, for values of empirical parameters varied between $\pm\sigma$. (a) Isoscalar parameters for symmetric nuclei, as a function of A. (b) Isovector parameters for the Sn isotopic chain, as a function of $(N-Z)/A$.

A. Exploring the parameter space

Because of the close similarity between the results obtained with the analytical mass model (see Sec. II B 2) and the ones using the full variational determination of the density profile of the ETF meta-functional (see Sec. II B 1), in this section we only use the analytical mass model, which is computationally very fast.

We begin with the minimum bias hypothesis: we choose a uniform prior distribution of empirical parameters in all dimensions as in Table I.

Next, we ask ourselves whether the average value of the empirical parameters can be modified, and their uncertainty domain reduced, by the constraint of reproduction of experimental binding energies.

The posterior distribution after application of the mass filter is given by

$$p(\{P_\alpha\},C_{\rm fin}) = \mathcal{N} w_{\rm filter}(\{P_\alpha\},C_{\rm fin}) \prod_{\alpha=1}^{N_p} g_\alpha(P_\alpha) g_C(C_{\rm fin}), \tag{34}$$

where $\mathcal{N}$ is a normalization, $N_p = 7$ stands for the number of saturation empirical parameters, and the functions g_α, g_C are the priors, here taken as flat distributions in the range $\langle P_\alpha\rangle - \sigma_\alpha \leqslant P_\alpha \leqslant \langle P_\alpha\rangle + \sigma_\alpha$. The standard choice for the filter function $w_{\rm filter}$ is given by the likelihood probability:

$$w_\chi(\{P_\alpha\},C_{\rm fin}) = \exp[-\chi^2(\{P_\alpha\},C_{\rm fin})/2], \tag{35}$$

with the χ^2 function defined as

$$\chi^2 = \frac{1}{N-N_p-1}\sum_{i=1}^{N}\left(\frac{E_{i,th}-E_{i,\,\rm exp}}{100A_i}\right)^2. \tag{36}$$

Here, energies are given in KeV, and the sum extends over all the symmetric nuclei with $10 \leqslant Z \leqslant 50$ and all the experimentally known isotopes of the semimagic elements with $Z = 20,28,50,82$ ($N = 3047$ in our calculation). The denominator corresponds to the systematic theoretical error, chosen so as to have $\chi^2_{\rm min} \approx 1$ over the parameter space sample [46]. The experimental error bar on the masses is always much smaller than the systematic theoretical error, and has been neglected.

To better visualize the effect of the filter and at the same time have a convenient representation of the average binding energy deviation associated with each parameter set, we also introduce a dimensional quantity analogous to the χ^2, which directly measures the average binding energy deviation over the symmetric nuclei as well as semimagic isotopic chains:

$$\Delta = \frac{1}{N}\sum_{i=1}^{N}\frac{|E_{i,th}-E_{i,\,\rm exp}|}{A}, \tag{37}$$

where the sum extends over the same nuclei as for Eq. (36).

We then define a filter function selecting those parameter sets for which $\Delta < \Delta_{\rm cutoff}$, where $\Delta_{\rm cutoff}$ is varied in order to observe the influence on the different observables as well as model parameters:

$$w_\Delta(\{P_\alpha\},C_{\rm fin}) = \Theta(\Delta_{\rm cutoff}-\Delta). \tag{38}$$

The corresponding posterior distribution p_Δ thus explicitly depends on the chosen value of $\Delta_{\rm cutoff}$, and so on the goodness requested from the models to reproduce the data.

Once the sample of models is filtered according to the chosen cutoff, centroids and standard deviations for any observable O can be calculated by integrating the posterior distribution p over the model parameters as

$$\langle O\rangle = \int dP_1\cdots dP_{N_p} dC_{\rm fin}\, O p(\{P_\alpha\},C_{\rm fin}), \tag{39}$$

$$\sigma_O^2 = \int dP_1\cdots dP_{N_p} dC_{\rm fin}[O-\langle O\rangle] p(\{P_\alpha\},C_{\rm fin}). \tag{40}$$

In these expressions, the value of the observable O in the integral is evaluated within the considered parameter set, $O \equiv O(\{P_\alpha\},C_{\rm fin})$, and p can be p_χ [using Eq. (36)] or p_Δ [if Eq. (38) is used]. We remark that O may or may not coincide with one of the model parameters $\{P_\alpha\}$, $C_{\rm fin}$.

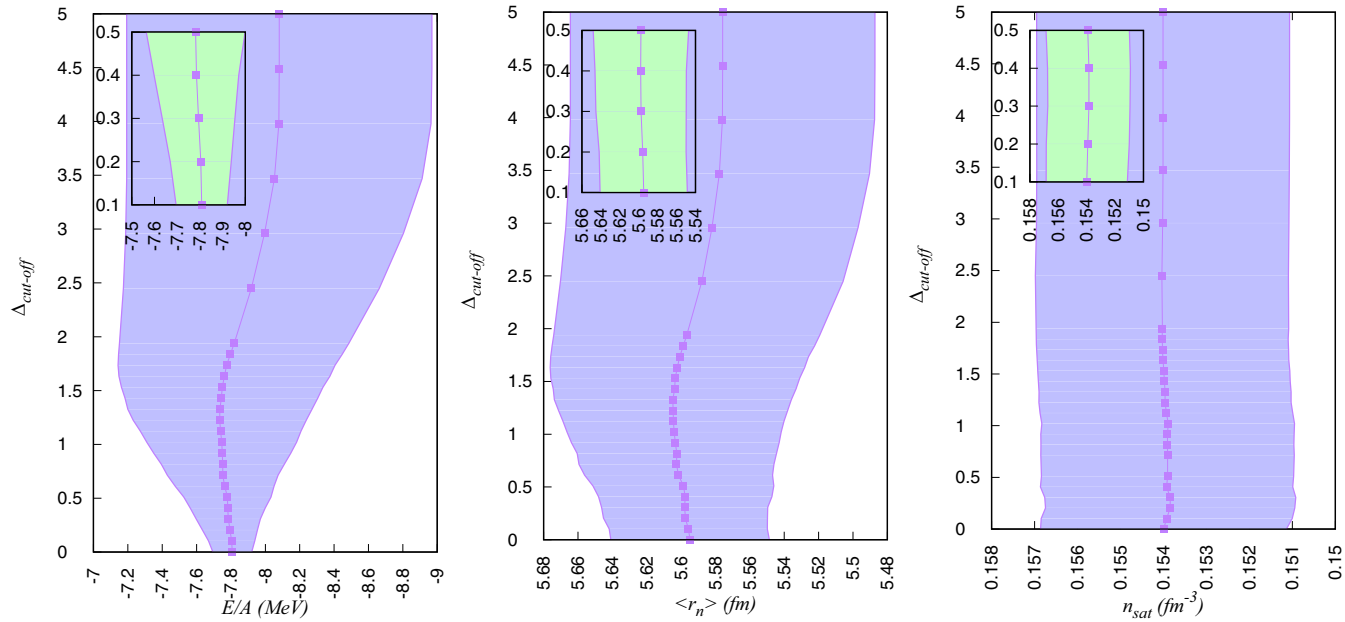

FIG. 4. Effect of cutoff in Δ on the average (central purple line) and standard deviation (band width) for two different observables—the ^{208}Pb binding energy per nucleon (left) and its neutron radius (center)—and the $n_{\rm sat}$ empirical parameter (right). In each panel, the inset shows the same for $\Delta_{\rm cutoff} < 0.5$.

B. Mean and variance

Using the cutoff filter w_Δ [Eq. (38)], we computed the mean and variance of some empirical quantities and observables, namely the binding energy per nucleon, rms neutron radius of ^{208}Pb, and saturation density $n_{\rm sat}$, shown in Fig. 4. For each panel, the centroid and standard deviation of the likelihood posterior distribution are additionally given in Table II.

In each of the panels, the lines indicate the mean value $\langle O\rangle$ and the values within a standard deviation of σ. The shown behaviors are representative of the general evolution with $\Delta_{\rm cutoff}$ of all the quantities we have examined. Specifically, all binding energies behave very similarly to the left panel of Fig. 4; all neutron and charge radii behave as in the central panel of Fig. 4; and all empirical parameters show a very constant behavior as in the right panel of Fig. 4. For all observables and model parameters, the average values only slightly evolve with $\Delta_{\rm cutoff}$, showing that our reference set is not far away from an optimized set. The variance of the energy per particle monotonically decreases, showing that $\Delta_{\rm cutoff}$ is indeed a measure of the quality of reproduction of individual binding energies. The variance of the radii also globally decreases. This is also expected because a smaller value of $\Delta_{\rm cutoff}$ corresponds to a reduction of the parameter space, and therefore of the possible variation among the different models. However we can see that the cutoff is ineffective starting at around $\Delta_{\rm cutoff} \approx 0.5$ MeV: a reproduction of the experimental binding energy better than 500 KeV per nucleon does not improve our uncertainty on the nuclear radius. Finally, the constant behavior of all the empirical parameters $\{P_\alpha\}$ is less expected. None of them (in average as well as in standard deviation) depends of the goodness requested in the reproduction of binding energies.

TABLE II. Centroid and standard deviation of the likelihood posterior distribution for the observables in Fig. 4.

Parameter	E/A (^{208}Pb) (MeV)	$\langle r_n\rangle$ (^{208}Pb) (fm)	$n_{\rm sat}$ ($\rm fm^{-3}$)
Average	−7.806	5.596	0.154
Standard deviation	0.124	0.046	0.003

This observation suggests that, if imposing a reproduction of the experimental binding energies, one cannot expect to be able to greatly reduce the uncertainty of the empirical parameters. This is due to the fact that the χ^2 hypersurface is relatively flat: all EoS parameters affect more or less in a similar way the nuclear binding energy (see Fig. 2). Since we are not supposing any *a priori* correlation among the parameters, compensations can freely occur. This is similar to the study of neutron stars, where compensation between different empirical parameters were observed to greatly reduce the effectiveness of the filters [21].

The only model parameter that can be better constrained by a better reproduction of nuclear mass is the finite size parameter $C_{\rm fin}$. This is shown in Fig. 5, which displays the evolution of the variance of $C_{\rm fin}$ with the cutoff (the average value is not affected).

However, the observed reduction of the standard deviation is essentially due to the fact that we have assumed a widely spread prior for this parameter. At a still relatively large value of the cutoff $\Delta_{\rm cutoff} \approx 0.25$ MeV, a convergence is observed for a non-negligible width, meaning that extreme values of $C_{\rm fin}$ are not excluded by the binding energy reproduction, because they can be compensated by the smaller but combined opposite effect of the EoS parameters.

The centroids and standard deviations obtained using the likelihood filter, Eq. (36), instead of the cutoff dependent one, Eq. (38), are given in Table II. These values are almost

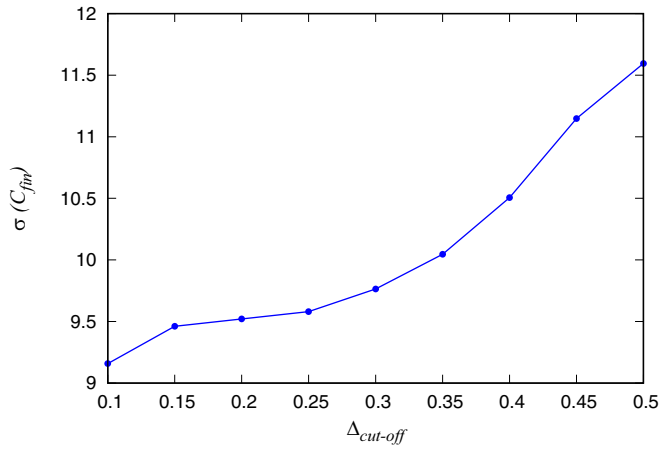

FIG. 5. Variance of the posterior distribution p_Δ of the finite size $C_{\rm fin}$ parameter as a function of the cut-off (see text).

identical to the ones obtained with the $\Delta_{\rm cutoff}$ filter for $\Delta_{\rm cutoff} \leqslant 0.5$ MeV.

To conclude, it appears from this study that an improvement in the predictive power of the mass model would not lead to any further constraint on the EoS empirical parameters besides the state-of-the-art values represented by Table I.

C. Correlations

We now come to the main result of this study, namely the search for physical correlations of the different empirical parameters among themselves, as well as with the radii and skins. In particular, the correlation coefficients between parameters and observables allows determination of the most influential observables in constraining the EoS [18,22–24]. They are defined as

$$c(X,Y) = \frac{\sigma(X,Y)}{\sigma(X)\sigma(Y)} = \frac{\langle (X-\langle X\rangle)(Y-\langle Y\rangle)\rangle}{\sigma(X)\sigma(Y)}, \qquad (41)$$

where X, Y denote parameters or observables, and the averages, variances, and covariances are computed on the posterior distribution.

The covariance study is done on the posterior distribution of empirical parameters with the binding energy filter given by Eqs. (35) and (36). We have checked that the use of the cutoff filter produces the same correlation matrix provided $\Delta_{\rm cutoff} \leqslant 0.5$ MeV.

To summarize the different correlations, we display in Fig. 6 the correlation matrix of the following quantities: empirical parameters ($n_{\rm sat}$, $E_{\rm sat}$, $K_{\rm sat}$, $E_{\rm sym}$, $L_{\rm sym}$, $K_{\rm sym}$), the effective mass m^*/m, the finite size parameter $C_{\rm fin}$, and some observables in ^{208}Pb, namely the rms charge radius $\sqrt{\langle r_{ch}^2\rangle}$, neutron rms radius $\sqrt{\langle r_n^2\rangle}$, neutron skin ΔR_{np}, and diffuseness a. The picture is qualitatively the same if other stable nuclei are chosen.

The first observation in this plot is that none of the empirical parameters (including the effective mass) are correlated to each other. In particular, the correlation coefficient between $L_{\rm sym}$ and $E_{\rm sym}$ is close to zero, at variance with numerous studies in the literature [4,10,15,16,47,48]. That correlation is generally explained by the fact [49] that nuclear structure probes the symmetry energy at densities below saturation: to have a given value for $e_{IV}(n_0 < n_{\rm sat})$, a higher (lower) value of $E_{\rm sym} = e_{IV}(n_{\rm sat})$ must be associated to a higher (lower) value of its derivative at $n_{\rm sat}$, namely $L_{\rm sym}$. However, this argument neglects the effect of the second derivative $K_{\rm sym}$. In Skyrme forces, $K_{\rm sym}$ is typically negative and strongly *a priori* correlated with $L_{\rm sym}$, therefore the argument holds. But if we allow a larger exploration of the $K_{\rm sym}$ parameter space, we can see that the new behaviors explored for the symmetry energy are still compatible with the binding energy constraint, and break the simple correlation between $E_{\rm sym}$ and $L_{\rm sym}$. This suggests that this commonly observed correlation is not a direct consequence of the constraint of mass reproduction, but might be due to the lack of flexibility of the Skyrme functional.

If we now turn to the correlations between observables and empirical parameters, apart from the trivial correlation between the neutron and charge rms radii, the strongest correlations visible in the plot are the correlations of the radii with the saturation density $n_{\rm sat}$, and that between the neutron skin ΔR_{np} and the slope of symmetry energy $L_{\rm sym}$.

The correlation of the radii with the saturation density $n_{\rm sat}$ is relatively trivial and expected, since the value of $n_{\rm sat}$ determines the average density of nucleons per volume. The constant $n_{\rm bulk}$ is indeed a function of the saturation density in our model and it explicitly enters in the definition of the radii. At low δ values, the second important quantity entering in the determination of the bulk density is $K_{\rm sat}$ [see Eq. (23)], which explains the weaker correlation between the radii and $K_{\rm sat}$.

The excellent correlation of ΔR_{np} with $L_{\rm sym}$ is in agreement with previous studies in the literature [18,22–24,37], which used specific Skyrme or RMF energy functionals. However, other correlations shown in the literature with $E_{\rm sym}$ or $K_{\rm sym}$ [14,50] are not observed here, which might again indicate the model dependence of these correlations.

The ΔR_{np}-$L_{\rm sym}$ correlation can be understood from the fact that the skin is proportional to the average displacement between neutrons and protons ΔR_{HS} [39], as can be seen from Eq. (33). Now, ΔR_{HS} is directly linked to the isospin dependence of the saturation density; see Eq. (25). This latter is determined by the ratio $L_{\rm sym}/(K_{\rm sat} + K_{\rm sym}\delta^2)$; see Eq. (23). The value of the bulk asymmetry δ is small in stable nuclei $\delta \approx 0.1$ and the parameter $K_{\rm sat}$ is relatively well constrained by the isoscalar giant resonance mode. As a consequence, $L_{\rm sym}$ is the key parameter to determine the neutron skin.

A word of caution has to be given here. In our analytical mass model we have employed the approximation $a_n = a_p$. Since the diffusivity depends in a complicated way both on the empirical parameters and on the finite size ones, this simplification might lead to an overestimation of the quality of the correlation. Still, it should be stressed that this same excellent correlation was observed also in a theoretical analysis where this approximation was not done [24]. Also, an analysis with the full ETF mass model, where $a_n(N,Z)$ and $a_p(N,Z)$ are independent parameters variationally determined for each nucleus, confirms the correlation between ΔR_{np} and $L_{\rm sym}$.

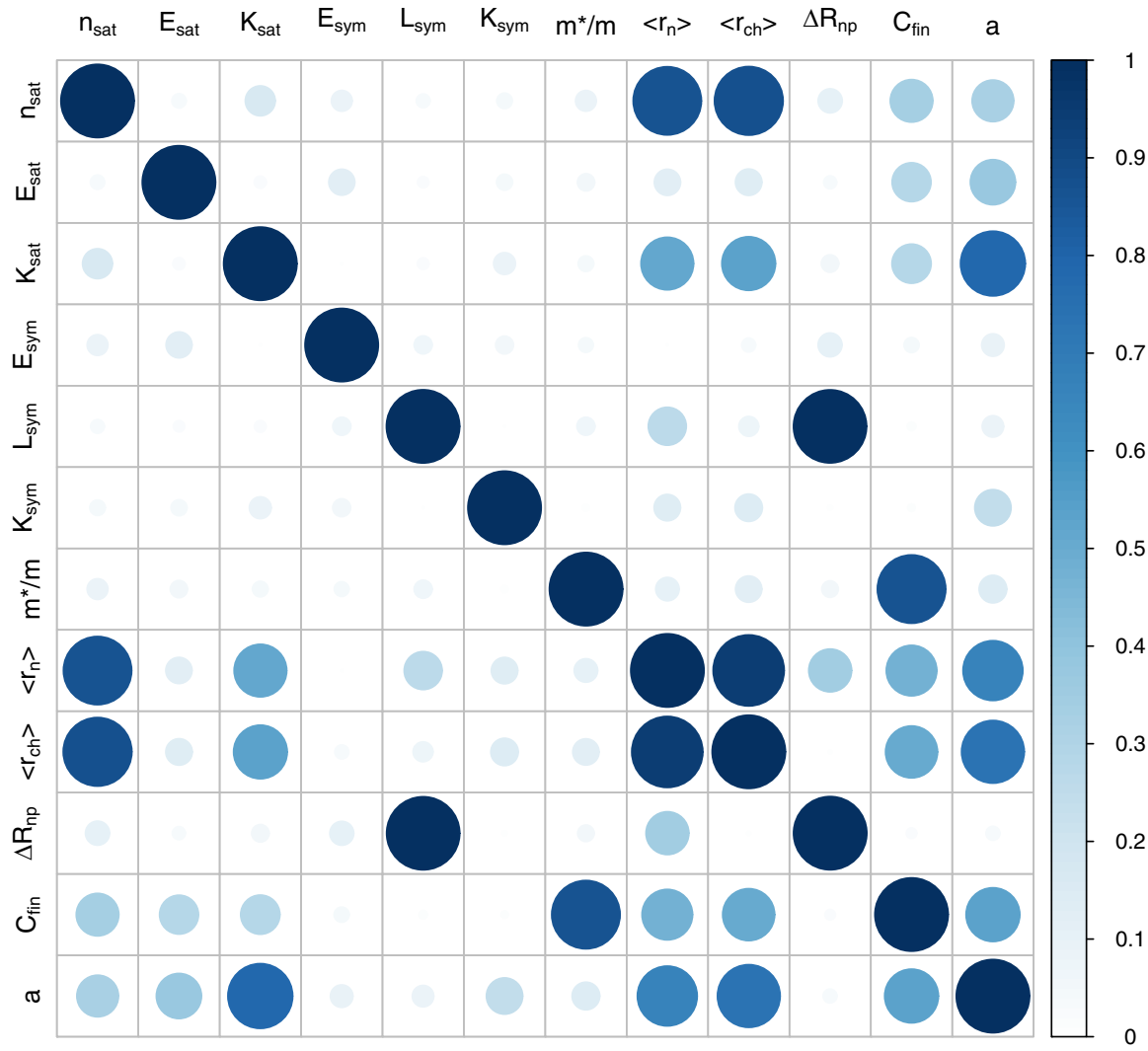

FIG. 6. Posterior correlation matrix for empirical parameters and nuclear observables, after application of the mass filter.

Finally, the parameters related to the nuclear surface exhibit different, though weak, interesting correlations. The finite size parameter $C_{\rm fin}$ is correlated to the effective mass and, in a weaker way, to the radii. This is consistent with our observation that $C_{\rm fin}$ and m^* are the two most influential parameters in the determination of the binding energy. A clear correlation is observed between $K_{\rm sat}$ and a. This is an interesting feature since these two quantities contribute to the surface energy: $K_{\rm sat}$ represent the bulk contribution while a is more complex. The parameter a is also found to be correlated with the radii r_{ch} and r_n, as is expected. Finally, a weak correlation is observed between a and $C_{\rm fin}$. This reveals the complex structure of the nonlinear terms in the ETF which depend on these parameters in a nontrivial way. In summary, surface terms induce some interesting correlations, but these correlations are weaker, and might be less robust, than the dominant correlation ΔR_{np}-$L_{\rm sym}$. Indeed the introduction of more gradient couplings and/or the introduction of an isovector diffuseness might change the properties of the surface parameters a, $C_{\rm fin}$ and their mutual correlations.

D. Radii and skins

We have seen in the previous section that constraints on $K_{\rm sat}$ and $n_{\rm sat}$ might come from the reproduction of nuclear radii, and constraints on $L_{\rm sym}$ could be obtained from the measurement of neutron skin. We therefore turn to examine the predictive power of our model on these observables in the present section.

The prediction of charge radii along the different semi-magic isotopic chains, obtained from the models filtered with the constraint of binding energy reproduction according to Eq. (38) (see Sec. IV A) is compared to experimental data from Ref. [51] in Fig. 7. In this figure, the experimental error bars are smaller than the size of the points. The predictions for the full ETF mass model with empirical parameters optimized on the binding energies (Table I) is also given, and seen to be compatible at the 2σ level with the analytical mass model.

We can see that the reproduction is not optimal, but the performance of the model is comparable to the one of complete ETF or DFT calculations in the absence of deformation [41,42].

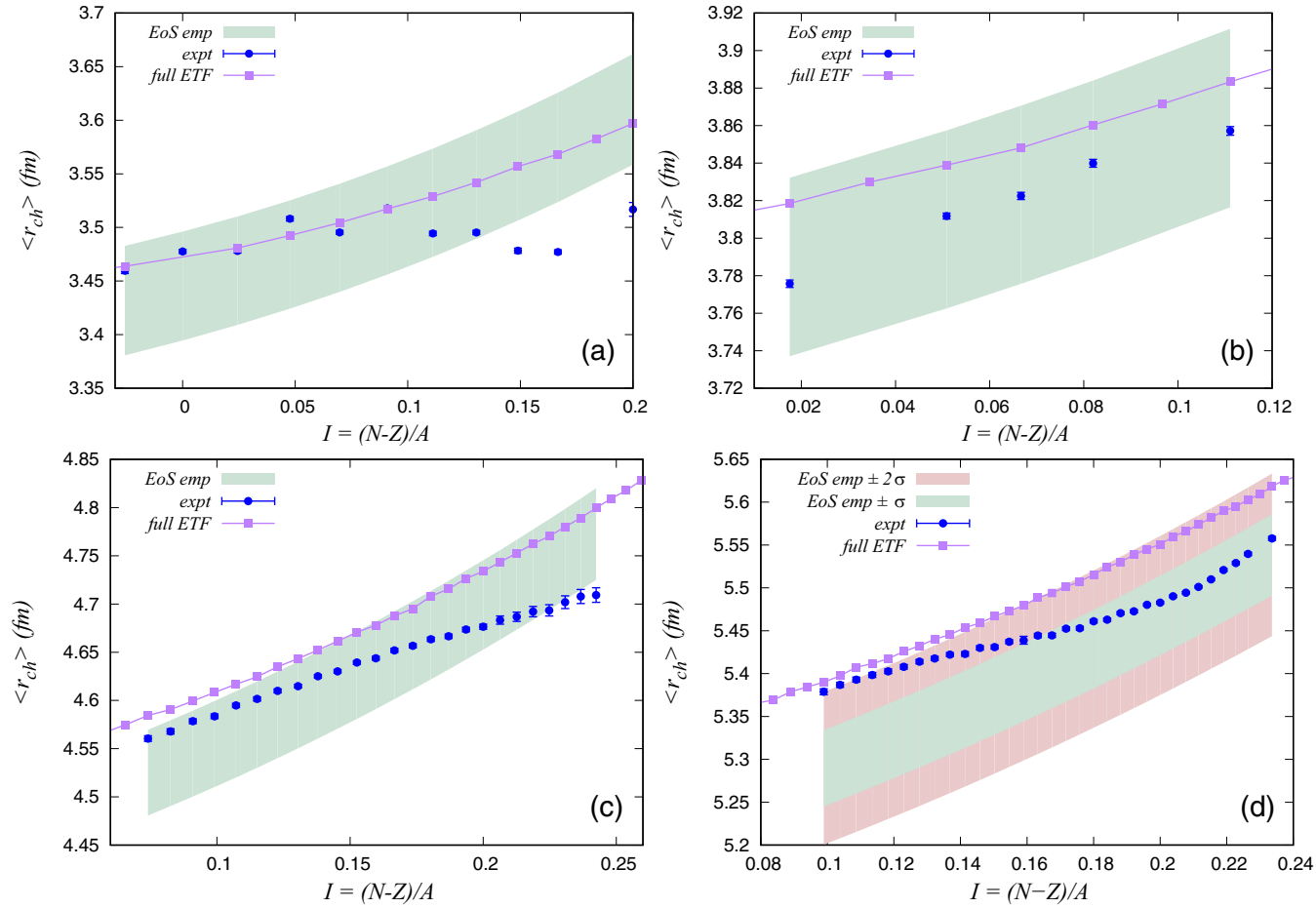

FIG. 7. rms charge radii vs I for semimagic isotopic chains for different Z values (a) 20, (b) 28, (c) 50, and (d) 82. Symbols with error bars: experimental data. Bands: predictions at 1σ (and 2σ) for the empirical EoS filtered through the binding energy constraint. Lines with filled squares: prediction from the full variational ETF with the optimized empirical parameter set.

Since the experimental error bars are much smaller than the theoretical ones, the charge radii constitute a very promising observable to further constrain the EoS. This is especially interesting for the $K_{\rm sat}$ parameter, for which some tension still exists [17] between constraints extracted from relativistic and nonrelativistic models.[1] It is highly probable that this tension might be induced by the different correlations between $K_{\rm sat}$ and $K_{\rm sym}$ in the two families of models [49,52], and could therefore be solved using the empirical EoS.

We have not attempted to put a further filter on the radii in the present study, because we consider that the present metamodeling is not sufficiently sophisticated for this purpose. Indeed, we can see from Fig. 6 that the radii also crucially depend, beside the EoS parameters, on the surface properties of the model (here a, $C_{\rm fin}$), which are treated in a simplified way in the present work. Moreover, the spherical approximation employed in this work is inadequate for many of the isotopes shown in Fig. 7. Finally, the small but systematic difference between the results of the analytical mass model and the full ETF with increasing nuclear charge suggests that it might be important to consistently include the Coulomb field in the variational theory for a correct description of charge radii. For these reasons, we leave the quantitative study of extracting EoS parameters from charge radii to a future work.

Next, we study the dependence of neutron skin ΔR_{np} on the global asymmetry parameter $I = (N - Z)/A$, for nuclei for which experimental measurements of the neutron skin exist [53]. We display the results in Fig. 8, along with the results from the full ETF calculation with the optimized empirical data set of Table I. It is clear from the figure that within the uncertainties of the empirical parameters, our model predicts neutron skins compatible with experimental results, with a comparable level of precision as complete ETF calculations [50].

This shows that a different diffuseness for the proton and neutron distribution is not necessary to reproduce the correct magnitude of the neutron skin, in contradiction with the results of Refs. [22,23,37]. We might understand this contradiction from the fact that our prescription for the diffuseness Eq. (24) effectively contains local and nonlocal isovector terms in a complex way, even assuming $a_n = a_p$.

Given the excellent correlation between the neutron skin and the $L_{\rm sym}$ parameter, we can expect that adding an

[1]For the reproduction of the same GMR observables, the nonrelativistic models prefer $K_{\rm sat} \approx 210$–240 MeV, while higher values $K_{\rm sat} \approx 250$–270 MeV are extracted from RMF calculations.

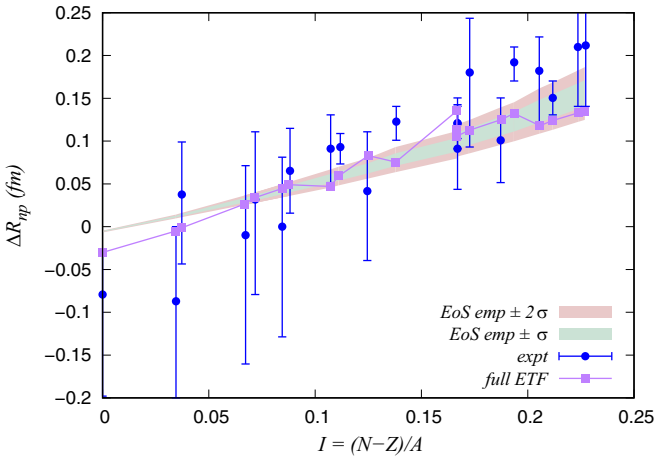

FIG. 8. Neutron skin as a function of global asymmetry for various nuclei. Symbols with error bars: experimental data. Bands: predictions at 1σ (and 2σ) for the empirical EoS filtered through binding the energy constraint. Lines with filled squares: prediction from the full variational ETF with the optimized empirical parameter set.

extra filter on the reproduction of the skin will allow us to considerably reduce the uncertainty interval on $L_{\rm sym}$ in a fully model-independent way. This study is not yet possible given the huge error bars of experimental data, but will hopefully be possible in a near future.

V. SUMMARY AND OUTLOOK

In this work we have developed a meta-modeling analysis of the correlations of the empirical parameters among themselves and with nuclear observables such as masses, radii, and neutron skins.

We used the extended Thomas-Fermi approximation at the second order in $\hbar$ and parametrized density profiles, to construct a fully analytical mass model for finite nuclei, based on a meta-modeling for homogeneous nuclear matter. The coefficients of this functional are directly related to the empirical parameters and can be independently varied, thus avoiding any artificial correlation induced by the chosen functional form. In finite nuclei, a single isoscalar extra parameter is required for the surface term to reasonably reproduce the experimental measurements of nuclear masses all along the nuclear chart. Our results show that no physical correlations exist among the different empirical parameters as far as the reproduction of binding energy is concerned, and thus suggest that the correlations shown in the literature might arise from the specific functional form assumed for the energy density, in particular for Skyrme functionals.

Charge radii exhibit interesting correlations both with EoS parameters ($K_{\rm sat}$ and $n_{\rm sat}$) and with the properties of the nuclear surface, which are less universal and might depend on the details of the variational theory. It will be interesting to try to disentangle these two aspects with dedicated calculations in the future.

We also showed that it is possible to reasonably reproduce the present measurements of neutron skins in nuclei even without the contribution from the differences in surface diffuseness between protons and neutrons. In agreement with some previous studies, we find that the neutron skin depends only on the slope of the symmetry energy $L_{\rm sym}$ and thus represent an extremely important observable to constrain the nuclear equation of state for astrophysical applications. This result stresses the importance of precise measurements of this key quantity in the next future [54,55].

ACKNOWLEDGMENTS

This work was partially supported by the NewCompStar COST action MP1304 [56]. D.C. acknowledges financial support from the CNRS and LPC. Discussions with L.Colo are gratefully acknowledged.

[1] M. Oertel, M. Hempel, T. Klahn, and S. Typel, Rev. Mod. Phys. **89**, 015007 (2017).
[2] B. A. Li, À. Ramos, and G. Verde *et al.*, Eur. Phys. J. A **50**, 9 (2014).
[3] J. M. Lattimer and M. Prakash, Phys. Rep. **621**, 127 (2016).
[4] M. B. Tsang, J. R. Stone, F. Camera, P. Danielewicz, S. Gandolfi, K. Hebeler, C. J. Horowitz, Jenny Lee, W. G. Lynch, Z. Kohley, R. Lemmon, P. Moller, T. Murakami, S. Riordan, X. Roca-Maza, F. Sammarruca, A. W. Steiner, I. Vidaña, and S. J. Yennello, Phys. Rev. C **86**, 015803 (2012).
[5] J. M. Lattimer and Y. Lim, Astrophys. J. **771**, 51 (2013).
[6] J. M. Lattimer and A. W. Steiner, Eur. Phys. J. A **50**, 40 (2014).
[7] M. Dutra, O. Lourenco, S. S. Avancini, B. V. Carlson, A. Delfino, D. P. Menezes, C. Providência, S. Typel, and J. R. Stone, Phys. Rev. C **90**, 055203 (2014).
[8] A. W. Steiner, J. Phys. G **42**, 034004 (2015).
[9] M. Fortin, C. Providência, Ad. R. Raduta, F. Gulminelli, J. L. Zdunik, P. Haensel, and M. Bejger, Phys. Rev. C **94**, 035804 (2016).
[10] M. Kortelainen, J. McDonnell, W. Nazarewicz, P.-G. Reinhard, J. Sarich, N. Schunck, M. V. Stoitsov, and S. M. Wild, Phys. Rev. C **85**, 024304 (2012).
[11] A. W. Steiner, J. M. Lattimer, and E. F. Brown, Astrophys. J. **722**, 33 (2010).
[12] A. Ayriyan, D. E. Alvarez-Castillo, D. Blaschke, and H. Grigorian, J. Phys. Conf. Ser. **668**, 012038 (2016).
[13] D. L. Smith, *Probability, Statistics, and Data Uncertainties in Nuclear Science and Technology* (American Nuclear Society, LaGrange Park, IL, 1991).
[14] W. Nazarewicz, P.-G. Reinhard, W. Satula, and D. Vretenar, Eur. Phys. J. A **50**, 20 (2014).
[15] C. Ducoin, J. Margueron, C. Providência, and I. Vidaña, Phys. Rev. C **83**, 045810 (2011).
[16] E. Khan, J. Margueron, and I. Vidaña, Phys. Rev. Lett. **109**, 092501 (2012); E. Khan and J. Margueron, Phys. Rev. C **88**, 034319 (2013).
[17] J. Margueron, F. Gulminelli, and R. Casali, arXiv:1708.06894.

[18] C. Mondal, B. K. Agrawal, M. Centelles, G. Colo, X. Roca-Maza, N. Paar, X. Viñas, S. K. Singh, and S. K. Patra, Phys. Rev. C **93**, 064303 (2016).
[19] J. P. Kleijnen, *Statistical Tools for Simulation Practitioners* (Marcel Dekker, New York, 1986).
[20] A. Gelman, J. B. Carlin, H. S. Stern, D. B. Dunson, A. Vehtari, and D. B. Rubin, *Bayesian Data Analysis*, 3rd ed. (Chapman & Hall, London, 2013).
[21] J. Margueron, F. Gulminelli, and R. Casali, arXiv:1708.06895.
[22] M. Warda, X. Viñas, X. Roca-Maza, and M. Centelles, Phys. Rev. C **80**, 024316 (2009).
[23] M. Centelles, X. Roca-Maza, X. Viñas, and M. Warda, Phys. Rev. C **82**, 054314 (2010).
[24] P.-G. Reinhard and W. Nazarewicz, Phys. Rev. C **93**, 051303(R) (2016).
[25] M. Kortelainen, T. Lesinski, J. Moré, W. Nazarewicz, J. Sarich, N. Schunck, M. V. Stoitsov, and S. Wild, Phys. Rev. C **82**, 024313 (2010).
[26] R. Jodon, M. Bender, K. Bennaceur, and J. Meyer, Phys. Rev. C **94**, 024335 (2016).
[27] A. Bulgac, M. McNeil Forbes, and S. Jin, arXiv:1506.09195; A. Bulgac, M. M. Forbes, S. Jin, R. N. Perez, and N. Schunck, arXiv:1708.08771.
[28] B. A. Brown, Phys. Rev. Lett. **85**, 5296 (2000).
[29] S. Typel and B. A. Brown, Phys. Rev. C **64**, 027302 (2001).
[30] J. Piekarewicz, J. Phys. Conf. Ser. **492**, 012008 (2014).
[31] T. Lesinski, K. Bennaceur, T. Duguet, and J. Meyer, Phys. Rev. C **74**, 044315 (2006).
[32] M. Onsi, A. K. Dutta, H. Chatri, S. Goriely, N. Chamel, and J. M. Pearson, Phys. Rev. C **77**, 065805 (2008).
[33] F. Aymard, F. Gulminelli, and J. Margueron, J. Phys. G: Nucl. Part. Phys. **43**, 045105 (2016).
[34] F. Aymard, F. Gulminelli, and J. Margueron, J. Phys. G: Nucl. Part. Phys. **43**, 045106 (2016).
[35] J. Treiner and H. Krivine, Ann. Phys. (NY) **170**, 406 (1986).
[36] P. Papakonstantinou, J. Margueron, F. Gulminelli, and Ad. R. Raduta, Phys. Rev C **88**, 045805 (2013).
[37] X. Viñas, M. Centelles, X. Roca-Maza and, M. Warda, Eur. Phys. J. A. **50**, 27 (2014).
[38] P. Danielewicz and J. Lee, Nucl. Phys. A **958**, 147 (2017).
[39] W. D. Myers and W. J. Swiatecki, Nucl. Phys. A **336**, 267 (1980).
[40] F. Aymard, F. Gulminelli, and J. Margueron, Phys. Rev. C **89**, 065807 (2014).
[41] F. Buchinger, J. E. Crawford, A. K. Dutta, J. M. Pearson, and F. Tondeur, Phy. Rev. C **49**, 1402 (1994).
[42] Z. Patyk, A. Baran, J. F. Berger, J. Dechargé, J. Dobaczewski, P. Ring, and A. Sobiczewski, Phys. Rev. C **59**, 704 (1999).
[43] G. Audi, M. Wang, A. H. Wapstra, F. G. Kondev, M. MacCormick, X. Xu, and B. Pfeiffer, Chin. Phys. C **36**, 1287 (2012); M. Wang, G. Audi, A. H. Wapstra, F. G. Kondev, M. MacCormick, X. Xu, and B. Pfeiffer, *ibid.* **36**, 1603 (2012).
[44] S. Goriely, N. Chamel, and J. M. Pearson, Phys. Rev. C **88**, 061302 (2013).
[45] E. Chabanat, P. Bonche, P. Haensel, J. Meyer, and R. Schaeffer, Nucl. Phys. A **635**, 231 (1998).
[46] J. Dobaczewski, W. Nazarewicz, and P.-G. Reinhard, J. Phys. G: Nucl. Part. Phys. **41**, 074001 (2014).
[47] P. Danielewicz and J. Lee, Nucl. Phys. A **922**, 1 (2014).
[48] J. D. McDonnell, N. Schunck, D. Higdon, J. Sarich, S. M. Wild, and W. Nazarewicz, Phys. Rev. Lett. **114**, 122501 (2015).
[49]] G. Colo, N. V. Giai, J. Meyer, K. Bennaceur, and P. Bonche, Phys. Rev. C **70**, 024307 (2004).
[50] M. C. Papazoglou and Ch.C. Moustakidis, Phys. Rev. C **90**, 014305 (2014).
[51] K. Marinova and I. Angeli, At. Data Nucl. Data Tables **99**, 69 (2013).
[52] G. Colo, H. Sagawa, S. Fracasso, and P. F. Bortignon, Phys. Lett. B **668**, 457 (2008).
[53] A. Trzcinska *et al.*, Phys. Rev. Lett. **87**, 082501 (2001).
[54] C. J. Horowitz, Z. Ahmed, C. M. Jen, A. Rakhman, P. A. Souder, M. M. Dalton, N. Liyanage, K. D. Paschke, K. Saenboonruang, R. Silwal, G. B. Franklin, M. Friend, B. Quinn, K. S. Kumar, D. McNulty, L. Mercado, S. Riordan, J. Wexler, R. W. Michaels, and G. M. Urciuoli, Phys. Rev. C **85**, 032501 (2012).
[55] C. M. Tarbert *et al.* (Crystal Ball at MAMI and A2 Collaboration), Phys. Rev. Lett. **112**, 242502 (2014).
[56] http://www.cost.eu/COST_Actions/mpns/MP1304.